AUT Journal of Electrical Engineering
10.22060/EEJ.2025.24863.5779

Advanced State of Health Estimation for Lithium-Ion Batteries Using Deep Learning and Feature Engineering

Negar Khalili[1], *Saeed Khankalantary[2], Ali Najafi Ardekany[3]

[1]Master degree, Electrical Engineering Department, K. N. Toosi University of Technology, Tehran, Iran

[2*]Assistant Professor, Electrical Engineering Department, K. N. Toosi University of Technology, Tehran, Iran (Corresponding Author, Email:" s.kalantary@kntu.ac.ir")

[3]Assistant Professor, Mechanical Engineering Department, K. N. Toosi University of Technology, Tehran, Iran

Abstract

Obtaining an accurate estimate of the state of health of a lithium-ion battery is important for its efficiency and stability, but it's hard because the aging processes are so complicated and non-linear. Deep neural networks and long short-term memory networks are powerful tools, but their potential is often not realized if the raw operating features fail to capture synergistic aging mechanisms. This article proposes a novel two-stage hybrid feature engineering methodology to address this constraint. In the first stage, the method uses a binary particle swarm optimization algorithm to look for a small set of important predictive features. In the second stage, the parsimonious subset is enhanced with a physics-constrained Electro-Thermal Interaction Feature that incorporates terminal voltage and temperature interaction stresses. The resulting feature set was subsequently utilized for the training and evaluation of both deep neural networks and long short-term memory networks models. Adding the electro-thermal interaction feature significantly improves the predictability of both models on the primary B05 cell, raising the R^2 value from about 0.93 to over 0.99. To assess generalizability, the framework was rigorously validated using a cross-battery approach on two additional cells (B07 and B055), where the models maintained high performance with an average $R^2 > 0.97$. The findings indicate that domain-knowledge-intensive feature engineering significantly influences performance more than the architectural decision between deep neural networks and long short-term memory networks, facilitating highly accurate and robust state of health predictions, which are crucial in advanced battery management systems.

Keywords: Deep Learning Algorithms, State of Health (SOH), Feature Engineering, Binary Particle Swarm Optimization (BPSO), Optimization[1]

[1] Declaration of Generative AI

To ensure the utmost clarity, seamless flow, and grammatical precision in this manuscript, we employed Grok 4, an advanced artificial intelligence model developed by xAI, during the revision process. This tool facilitated the refinement of sentence structures, elimination of redundancies, and enhancement of logical progression without altering the original content or scholarly intent, thereby upholding the integrity of the research while promoting readability for a professional audience.

1. Introduction

Lithium-ion batteries (LIBs) possess substantial energy density, exhibit prolonged longevity, and demonstrate superior performance throughout utilization. These are some of the reasons why so many modern gadgets, such electric cars (EVs), mobile electronics, and renewable energy storage plants, use them [1-3]. Batteries are becoming more and more important to the world's energy patterns every day, so we need better ways to make sure they perform effectively and stay stable. SOH is undoubtedly a key diagnostic metric monitored by a battery management system (BMS). It shows how much power the battery has right now compared to how much power it was supposed to have when it was new. It provides a reliable indicator of its degradation and aging over time [4-6].

Electrochemical side reactions, mechanical and thermal stress, and changes in the environment are only a few of the many linked physicochemical factors that affect LIB aging [7, 8]. Charging and discharging in cycles and changing load conditions additionally speed up these processes. This causes the battery to lose performance in a way that is usually nonlinear and dynamic [9]. It is challenging for traditional modeling methods to capture this type of degradation process. Coulomb counting and electrochemical impedance spectroscopy, while relatively simple, frequently encounter drawbacks due to cumulative error, experimental complexity, and the requirement for proprietary equipment [10, 11].

To overcome the previously described constraints, data-driven strategies have surfaced as significant contenders for the SOH prediction [12]. These approaches utilize externally measurable values such as voltage, current, temperature, and capacity. These measurements are also straightforward to obtain during regular battery operation, reducing the need for detailed knowledge of internal electrochemical behavior [13-15]. LSTMs and DNNs are two examples of deep architectures that have shown a lot of promise in their ability to acquire long-term temporal patterns from battery operational data. In addition, Models have shown a significant improvement over standard machine learning methods for predicting Remaining Useful Life (RUL)[16-18].

But how well any data-based model can make predictions always depends on how well its input features represent the data and how accurate they are. Feature selection algorithms can use data to determine a decent set of characteristics, but these sets of raw features seldom take into consideration the subtle, synergistic correlations that cause batteries to wear out. For example, it is widely recognized that the influence of temperature on battery degradation is more pronounced under high voltage and current conditions. When we look at these parameters by themselves, we can't observe this simple non-linear relationship [19-21].

This paper presents a novel hybrid feature engineering technique designed to enhance the reliability and accuracy of SOH estimate, motivated by these observations. There are two steps in the new process. To start, a BPSO procedure is utilized to acquire a tiny yet useful collection of features from the initial set of features. In the second stage, a physics-based Electro-Thermal Interaction Feature (ETIF) is introduced to this modest set of features. The ETIF's purpose is to copy the effects of both electrical and thermal stress. After that, we use this better collection of features to train and evaluate LSTM and DNN models. This helps us see how these engineering features affect different deep learning paradigms.

This work offers fundamental contributions to the assessment of LIB health. This study introduces and analyzes an innovative two-stage feature engineering process that combines physics-constrained feature enhancement through ETIF with feature reduction via BPSO. Second, systematic comparative tests demonstrate that the proposed hybrid strategy substantially enhances SOH prediction capabilities of both LSTMs and DNNs models, underscoring the paramount significance of knowledge-informed feature design relative to model structure selection. Third, it is suggested to execute a comprehensive feature importance analysis to confirm the predictive efficacy of ETIF and to promote clearer and more reliable implementations of BMS.

This paper is organized as follows: In Section 2, we present a brief summary of the previous researches on approaches for predicting SOH. Section 3 goes into information about the data, the proposed method, and the model structures. Section 4 demonstrates the findings of the experiments, how they compare to

each other and, the results are critically analyzed. In Section 5, conclusion, the main accomplishments of this research and their engineering implications are summarized.

2. Related works

Lithium-ion batteries are common in modern technology, powering devices from electric cars to cell phones. To ensure they function as required, reliably and safely, it is essential to accurately forecast their SOH. SOH is the ratio of the current to original capacity and is time-dependent, which declines over a duration of continuous alterations due to a number of factors such as charge-discharge cycles, temperature, and chemical degradation (Shen et al. [22]). It is imperative to calculate the amount of SOH and RUL accurately due to the so-called battery's inherent variability in electrochemical process, varying operation conditions over their life cycle, and computation time-trades towards constructing high accuracy predictions (Zhao et al. [23]). This paper presents an overview of the recent developments in SOH prediction techniques and names some of the techniques that consist of incremental capacity analysis, multi-dimensional health indicators, future load information use, and use of different machine learning models.

Battery operating statistics-based feature extraction has been the most widely used SOH estimation method. Wen et al. [24] develop a SOH prediction model according to an IC curve feature and backpropagation neural networks. It has pertinent discussion of IC curve behavior and SOH correlation analysis based on temperature-based mapping correlation on a least square's basis. It further includes an online real-time correction predicate mode based on always-current characteristic data to provide higher accuracy across broad aging phases. Jia et al. [25] also include discussion regarding issues with the estimation of SOH when relying on direct capacitance measurement online. This led them to identify indirect health indicators derived from voltage, current, and temperature profiles during charge and discharge. They use grey relational analysis and Gaussian Process Regression to extract relevant IHIs which relate with SOH predictions using a number of annual observations. Other than that, they also illuminate the achievement of high predictive accuracy using three IHIs and accessible SOH values to predict RUL. Yu et al. [26] introduce novel health indicators for battery equivalent circuit model and constant current discharge curves, such as polarization resistance, polarization capacitance, initial discharge resistance, and equal voltage drop discharge time. It also prefers multi-dimensional health indicator (HI) strategy adoption, which, compared to the adoption of single HI input type mode, is extremely precise with the use of PSO and LSTM. In addition, Peng et al. [27] present the first SOH estimation methods through characteristic fusion and earth-based method through interval voltage selection. The paper suggests a sampling time and feature correlation-based voltage interval selection methodology that minimizes practically the training data needed. It further suggests a double correlation similarity examination employed in its initial stages for SOH prediction, along with a feature fusing approach utilizing entropy weights and correlation characteristics for alleviating redundancy. It shows excellent prediction ability with coefficients of determination greater than 0.98.

Forward and dynamic data incorporation have contributed much, aside from static property retrieval. Qian et al. [28] observed a limitation that may be prevalent in most data-driven techniques, which simply rely on past data. They suggest a new method for forecasting the SOH using future-load information and historical information with an attention-based multisource sequence-to-sequence model. The model has two encoders and a decoder, and also utilizes attention mechanisms, thereby being able to effectively cope with global dependencies and make trustworthy long-term SOH predictions under most load and ambient temperature conditions, thereby being robust to different start points of prediction as well as different lengths of input.

Machine learning algorithms and deep learning architectures are the fundamental components of the enhanced techniques employed in predictive analysis. Shu et al. [29] give an extensive survey of machine learning-based SOH estimation. They categorize several methods, unite feature extraction techniques appropriate for health, and compare various machine learning approaches. Their research

gives a series of models' benefits and limitations, accuracy, and parameters of the algorithms. Tang et al. [30] suggest a high-performance multivariate dimensionality-reduction method integrated into a Bayes-optimized bi-directional long short-term memory algorithm, specifically to be employed in the SOH estimation and RUL prediction. They use discharge data health indicators, collaborative dimensionality reduction via Pearson correlation, and Bayesian search strategy for determining the optimal hyperparameters of bi-directional long short-term memory, which makes it more precise and trustworthy. Table 1. summarizes the applications of some of the studies of feature engineering using advanced techniques and deep learning models to predict SOH and RUL. It indicates the methodology they employed, the model employed, and the accuracy attained.

Table 1.Summary of the different approaches for applying feature engineering and deep learning to SOH and RUL prediction.

Study	Feature Engineering Approach	Model Used	Best Reported Error
Pepe & Ciucci (2023) [31]	Charge-discharge profile features, saliency & Pearson analysis	LSTM, GRU with custom loss	SOH: 5.49%, EOL: -1.27%
Wang et al. (2023) [32]	Three-step construction & filter/embedded feature selection	XGBoost, LightGBM, Random Forest	RMSE < 0.29%, Max error < 1%
Zhao et al. (2023) [33]	Direct, evolution, statistical features with filtering	Sparse Autoencoder + Transformer	RUL error: 2.6% (100 cycles)
Zhang et al. (2023) [34]	Multidomain fusion (time, freq., entropy) + CatBoost + SSA	CatBoost optimized with Sparrow Search	RMSE < 0.02, $R^2 \geq 0.98$
Bian et al. (2025) [35]	Hierarchical IC & charge-discharge feature stacking + PSO	PSO-MLSt-LSTM (stacked model)	RMSE: 0.0035–0.0078
Shu et al. (2020) [36]	Charging voltage curve-based feature optimization	Fixed-size LS-SVM + Genetic Algorithm	<2% SOH error
Jorge et al. (2022) [37]	Sliding window time series feature extraction	LSTM (window-based)	Long-term accurate prediction (no %)
Jiang et al. (2022) [38]	Convolutional autoencoder + self-attention	Autoencoder + Self-attention	RMSE: 0.0048, MAPE: 0.46%

3. Methodology

This section talks about the new and better management that individuals check the level of SOH in lithium-ion batteries. There are five main steps to take, such getting and cleaning the data, figuring out how the model works, and choosing the performance metrics. The model for the investigation is shown in Fig. 1.

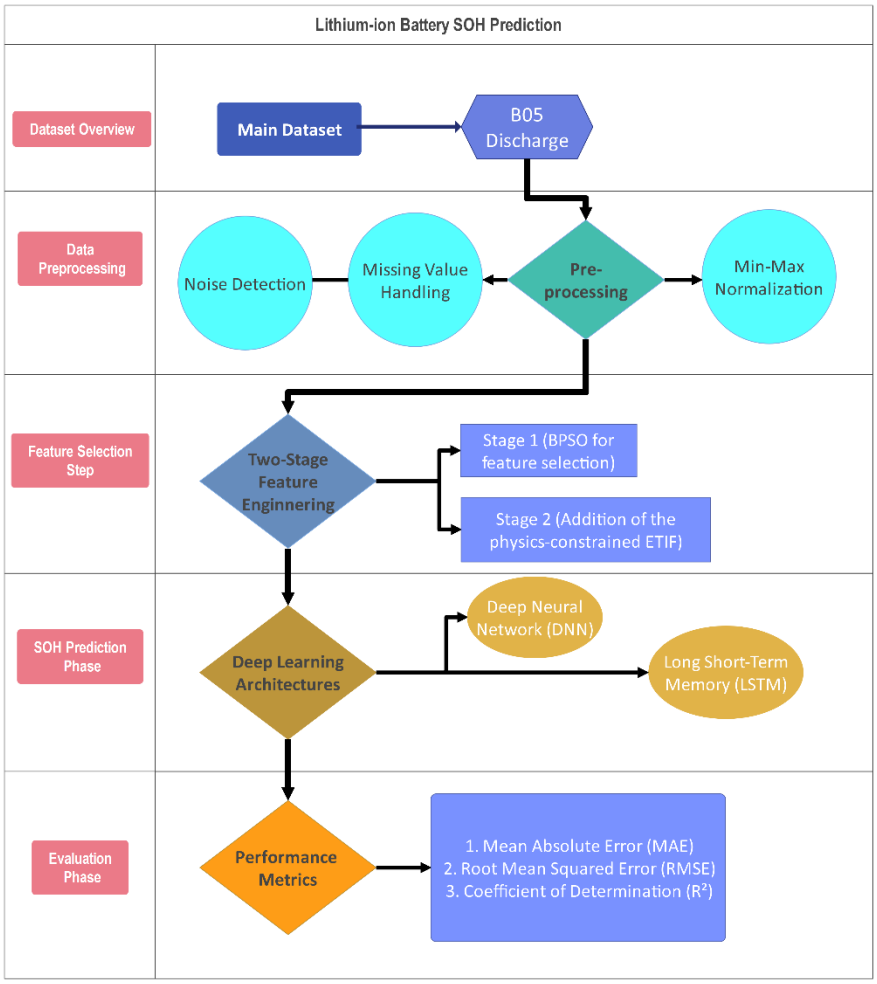

Fig. 1 Overview of the proposed methodology, highlighting the two-stage feature engineering process. It shows the crucial phases, such getting the data and testing the final model.

3.1 Data Description

The data was obtained from the open-source NASA Ames Prognostics Center of Excellence Lithium-Ion Battery Dataset, a repository for prognostics and health management research [39]. This benchmark data set included a number of different ways to quantify battery degeneration. These were recorded in tightly controlled lab tests. For cycling tests on industrial lithium-ion batteries, the data were accumulated very systematically and intentionally at routine intervals until end-of-life conditions for the cells were achieved. This comprised measurement of operational Factors such as charge and discharge current, voltage, temperature, and capacities. Including time-series measurement of discharging, the dataset provides ample information regarding dynamics of battery ageing over time. For this research, three batteries from the main group of datasets were initially considered: B05, B07,

and B055. As illustrated in the Fig. 2, all three batteries exhibited a highly similar pattern of State of Health (SOH) degradation over cycles. Given this strong similarity in their degradation trends, and to avoid redundancy in the analysis, the study proceeds with a focused investigation using a single, representative cell: battery B05**.** The dataset for B05 consists of nine attributes: eight independent features (terminal_voltage, terminal_current, temperature, charge_current, charge_voltage, time, capacity, cycle) and one dependent variable, SOH, obtained by current capacity divided by initial capacity. Capacity is included as an independent feature as it is a directly measured parameter that contributes to modeling degradation dynamics, while SOH is the computed target. SOH retains estimation as its primary interest and subject of analysis. Descriptions of attributes have been provided for listed data, used here, in Table 2.

Table 2. Overview of Battery Discharge Datasets Used in This Study

Dataset Name	No. of Cycles	Initial SOH (%)	Final SOH (%)	Data Type
B05	168	0.9282	0.6437	Discharge
B07	168	0.9455	0.7002	Discharge
B055	168	0.9282	0.6437	Discharge

These sets of data typically include the primary battery characteristics measured through controlled charge and discharge tests, as demanded for SOH assessment. The primary characteristics usually include:

1. terminal_voltage: The voltage across the battery terminals during operation, which reflects the electrical potential and is key to assessing discharge/charge states.
2. terminal_current: The electric current flowing through the terminals of the battery. It will be positive (charging) or negative (discharging), giving an indication of the health of the battery.
3. Temperature: Shows the battery's outside or inside temperature at regular intervals. This can have a huge effect on how well the battery works and how long it lasts.
4. charge_current: The amount of electrical current that flows to the battery while it is charging, commonly measured in volts.
5. charge_voltage: The voltage used to charge the battery, which affects how well it works.
6. Time measurement: This tells us how long it takes to collect data, usually in seconds from the start of the experiment.
7. capacity: Battery capacity, measured in ampere-hours (Ah), represents the amount of charge a battery can deliver.
8. cycle: Number of discharge and charge cycles the battery has been put through; one complete discharge and one complete charge typically equal one complete cycle.
9. state of Health (SOH): The health of the battery, typically given as a percentage that measures the battery's ability to store and deliver energy compared to when it was newly installed. We care most about this measurement.

Prior to the construction of the model, the data had been preprocessed to ensure it was good, accurate, and consistent in its analysis. We started off by examining the dataset to check for any missing values within any of the most important features. We confirmed the dataset contained no missing values, thus eliminating the need for imputation or removal of rows.

10.22060/EEJ.2025.24863.5779

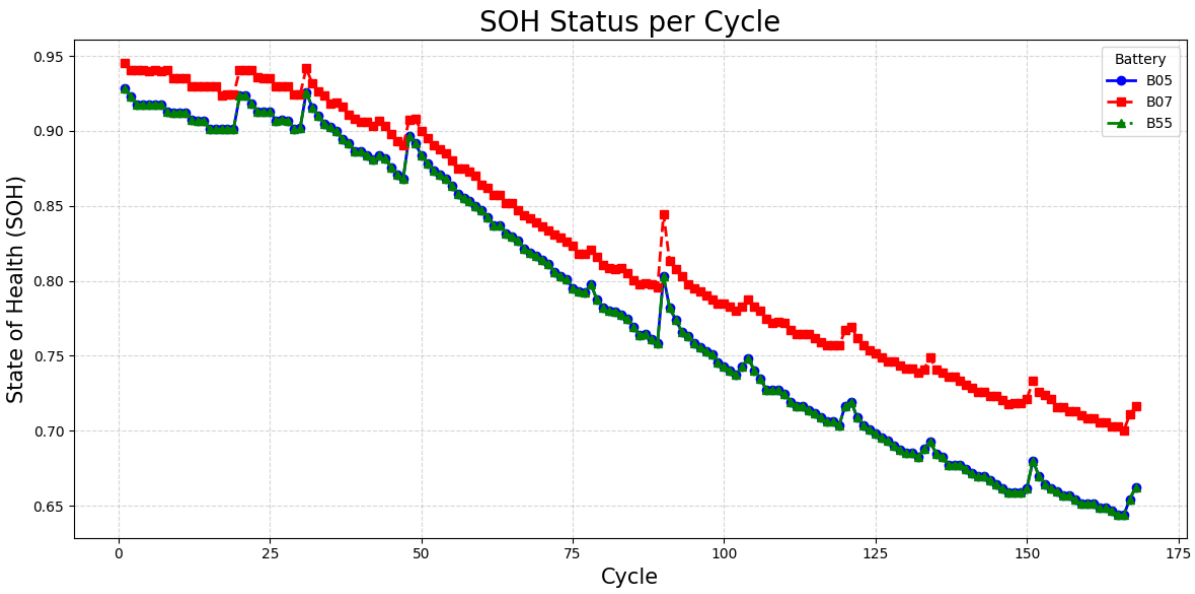

Fig. 2 SOH degradation over operational cycles for all batteries.

Fig. 2 shows the State of Health (SOH) degradation trends for three batteries, B05, B07, and B055, across 168 cycles. The figure reveals a strong similarity in their aging patterns, all exhibiting a characteristic non-linear decline from an initial SOH above 0.90 to a final SOH below 0.70. The degradation is not a simple straight line; it is marked by complex, short-term recovery spikes (visible as upward jumps) superimposed on the long-term downward trend. This combination of a steady decline with sporadic, non-linear recovery events highlights the dynamic nature of battery aging. Again, we should mention that given the high similarity in the degradation patterns of B05, B07, and B055, the analysis in this study is focused on a single, representative cell, B05, to avoid redundancy.

We applied min-max normalization to all numerical features to facilitate comparison and improve model convergence. Eq. (1) explains how the process changes each feature to fit within the range [0, 1]:

$$X_{Normalized} = \frac{X - X_{Min}}{X_{Max} - X_{Min}} \quad (1)$$

This kind of normalization keeps the shape of the distribution but eliminates the effect of features being in various scales (e.g., [degrees Celsius] and temperature), beneficial particularly in models that make use of gradients.

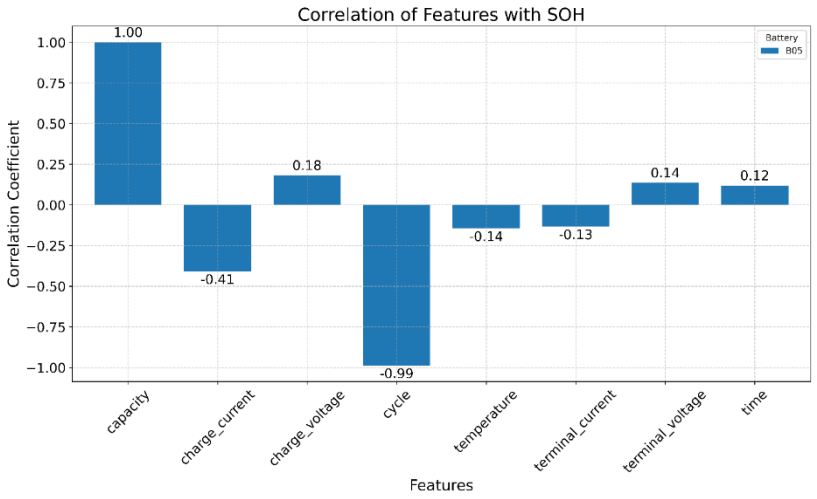

Fig. 3 Correlation coefficients between the SOH of battery B05 and different operational parameters.

From Fig. 3, we can observe that Pearson correlation coefficients between the SOH of battery B05 and different operational parameters, exhibit linear relationships that govern battery degradation. Unsurprisingly, capacity has a perfect positive correlation of 1.00, as SOH is directly derived from it. Cycle is the most predictive characteristic, having a very high negative correlation of -0.99, as predicted, reinforcing that successful cycles are the best linear prediction of the aging process. Charge_current is moderately negatively correlated at -0.41, with increased charging currents being related to increased health degradation. On the other hand, the remaining operational parameters, i.e., charge_voltage (0.18), terminal_voltage (0.14), time (0.12), temperature (-0.14), and terminal_current (-0.13), are all weakly linearly correlated with SOH. This implies their individual contributions are limited, justifying the need for higher-order features capable of modeling nonlinear dynamics and interactions among these variables.

3.2 Binary Particle Swarm Optimization (BPSO) Feature Selection

While feature engineering generates potentially useful predictors, not all features contribute equally to the model's predictive capability. The existence of irrelevant or redundant features may cause the curse of dimensionality, boost model complexity, add noise, and raise overfitting risk. Therefore, a rigorous feature selection process is essential. This research evaluated the application of a wrapper-based feature selection approaches using the BPSO algorithm to determine the best subset of independent variables which will give the highest predictive accuracy at the lowest model complexity.

In feature selection, the PSO algorithm is modified to run in a binary search space. Every particle in the swarm is a potential feature subset. Its position, x_i, is a D-dimensional binary vector, where D is the number of original and engineered features. A '1' in the *j-th* coordinate of the vector means that the *j-th* feature is selected and a '0' means it's not being selected.

Particle movement here in this binary space is based on their updated velocities, which are the probabilities of including a feature into the optimal subset. Though the velocity update equation is the same as in the basic PSO, given by Eq. (2). However, the position update is altered and the continuous velocity value is mapped to a probability interval [0, 1] by using a sigmoid function as defined in Eq. (3), and then used to decide the binary value of the new position.

1. **Velocity Update (same as standard PSO):**

$$v_{ij}(t+1) = w \,.\, v_{ij}(t) + c_1 \,.\, r_1 \,.\, (p_{best_{ij}}(t) - x_{ij}(t)) + c_2 \,.\, r_2 \,.\, (p_{best_j}(t) - x_{ij}(t)) \quad (2)$$

Where:

$v_{ij}(t)$ is the velocity of particle i in dimension j at iteration t.

w is the inertia weight.

c_1 and c_2 are the cognitive and social acceleration coefficients, respectively.

r_1 and r_2 are random numbers uniformly distributed in [0, 1].

$p_{bestij}(t)$ is the best position (feature subset) ever found by particle i in dimension j up to iteration t.

$g_{bestij}(t)$ is the best position (feature subset) ever found by the entire swarm in dimension j up to iteration t.

$x_{ij}(t)$ is the current position of particle i in dimension j at iteration t.

2. **Position Update (probabilistic):** A sigmoid function is applied to the new velocity to get a probability:

$$S\left(v_{ij}(t+1)\right)=\frac{1}{1+e^{-v_{ij}(t+1)}} \tag{3}$$

Where:

$S(v_{ij}(t+1))$ is the sigmoid-transformed velocity, representing the probability of the feature being selected.

The new position (i.e., whether to select a feature) is then determined by comparing this probability to a random number according to Eq. (4):

$$x_{ij}(t+1)=\begin{cases} 1 & if\ \ rand(\ ) < S\left(v_{ij}(t+1)\right) \\ 0 & Otherwise \end{cases} \tag{4}$$

where *rand ()* is a random number generated from a uniform distribution in [0, 1].

The fitness function is one of the essential parts of this wrapper algorithm, which has to reconcile two competing requirements: maximizing model predictive accuracy and minimizing the number of features selected. We create a composite fitness function in Eq. (5) to direct the BPSO search:

$$Fitness(x)=\alpha.\ Error(x)+(1-\alpha)\ .\ \frac{|x|}{D} \tag{5}$$

Where:

x is the binary feature subset vector of a particle.

Error(x) is the Root Mean Squared Error of the Deep Learning models when tested and trained on the feature subset formed by *x* alone.

$|x|$ is the number of features selected in the subset (i.e., the number of '1's in the vector).

D is the number of features available.

α is a weight parameter between [0, 1] to balance prediction accuracy and feature reduction. The value of α is increased to attach greater importance to minimizing model error, and the value of α is decreased to enhance the importance of choosing a more concise feature set.

BPSO-based feature selection is a systemized and iterative process. The algorithm begins by randomly initializing a swarm of particles where the binary position vector of each particle serves as an initial candidate feature subset. In each iteration, the algorithm calculates the fitness of each particle (Eq. (5)). This is done by training and cross-validating the LSTM model on the given feature subset specified by the current position of the particle and then determining its performance on the multi-objective fitness function.

According to this fitness value, all the particles refresh their memory of their individual best position (p_{best}), and the global best position of the swarm (g_{best}) is refreshed by finding that particle where the best fitness up to now was achieved. These global and local best positions subsequently control the motion of the swarm since the position and velocity of all particles are modified based on the BPSO equations, thereby pushing them towards better regions in the solution space. The iteration is repeated until a stopping criterion, for example, the maximum number of iterations predetermined or the achieved stable global best fitness value, is reached. At termination, the optimal feature subset is chosen as the global best particle position, (g_{best}). After that, this streamlined and minimized set of variables is used to make the final, better SOH prediction model.

3.3 Sensitivity Analysis of the Weighting Parameter α

A sensitivity analysis was conducted to evaluate the impact of the fitness function's weighting parameter, α, which balances the importance of model accuracy against the size of the feature subset. The parameter α was varied from 0.5 to 0.95 in increments of 0.1. The results, summarized in Table 3, indicate a key finding: for the battery dataset under study, the BPSO algorithm consistently identified the same optimal subset of four features—charge_current, charge_voltage, capacity, and cycle—regardless of the α value. This consistency underscores the fundamental importance of these particular operational parameters for estimating SOH.

While the feature subset size remained stable, the value of α had a pronounced effect on the optimization cost, which is heavily influenced by the model's RMSE. As α increased, giving greater priority to prediction accuracy, the best cost found by the BPSO decreased monotonically. This demonstrates that a higher α successfully guided the optimization process towards superior model performance. Consequently, $\alpha = 0.95$ was selected for the final model as it achieved the lowest possible error without altering the parsimonious feature set, thereby optimally balancing the objectives of the fitness function for this application.

Table 3 Sensitivity Analysis of the α Parameter on Feature Selection and Optimization Cost

α Value	Best Cost	Number of Selected Features	Selected Features
0.50	1.178	4	charge_current, charge_voltage, capacity, cycle
0.60	1.014	4	charge_current, charge_voltage, capacity, cycle

0.70	0.849	4	charge_current, charge_voltage, capacity, cycle
0.80	0.685	4	charge_current, charge_voltage, capacity, cycle
0.90	0.520	4	charge_current, charge_voltage, capacity, cycle
0.95	**0.438**	4	charge_current, charge_voltage, capacity, cycle

3.4 Introducing Electro-Thermal Interaction Feature (ETIF)

A new feature was engineered from the raw sensor data to help the model learn more complex patterns of battery degradation. Feature engineering is a key step in getting the data ready because it lets us build higher-level representations that can find hidden correlations and improve the efficiency of the model.

This engineered feature, defined in Eq. (6), is motivated by the interaction between temperature and terminal voltage. The concept behind this feature is that the combined effect of internal temperature and voltage stress is a key element of how batteries age and lose their SOH. High temperatures, especially when combined with high voltages, can speed up the decomposition of chemicals. This combination captures the synergistic effect of electrochemical and thermal stress on battery degradation. This interaction component lets the model figure out nonlinear effects that might not be clear if voltage and temperature are considered separately.

$$ETIF = v_{current\_terminal} \times Temperature \tag{6}$$

Incorporating this feature enriches the dataset with a representation more directly linked to the physicochemical processes of lithium-ion battery aging. The engineered feature was used in conjunction with the initial readings when training and testing the model.

The multiplicative form $V * T$ was chosen to capture the synergistic acceleration of degradation under high voltage and temperature, as supported by literature showing multiplicative effects on SEI growth and lithium plating [40, 41]. For example, Waldmann et al.[40] demonstrated that degradation rates increase with temperature at high SOC (linked to voltage), while Ramadass et al.[41] highlighted voltage-temperature interactions in capacity fade. Alternative nonlinear combinations were tested, including logarithmic ($log\ (V * T)$) and exponential ($exp\ (V / T)$). The simple product yielded the best performance, as summarized in Table 4.

Table 4 Comparison of ETIF Formulations on Model Performance (LSTM model)

Formulation	R^2 Score	RMSE
$V * T$	0.9909	0.0087
$log\ (V * T)$	0.91	0.012
$exp\ (V / T)$	0.92	0.014

3.5 Model Architecture

To compare the performance of deep learning techniques for SOH forecasting, two neural network architectures were employed: a DNN and an LSTM network. Both were chosen for their complementary strengths: DNNs for learning static feature representations, and LSTMs for capturing temporal dynamics in time-series data. Both were learned from the same input features chosen by PSO, raw sensor measurements and the engineered feature described in Section 3.3.

3.5.1 Hyperparameter Selection

Hyperparameters were optimized via grid search on a validation set (20% of training data), testing layers (1-3), units/neurons (16-512), learning rate (0.0001-0.01), dropout (0.1-0.5) and so on. The configuration minimizing validation MSE was selected. Results of the grid search are summarized in Table 5.

Table 5 Grid Search Summary for Optimal Hyperparameters

Parameter	DNN Optimal	LSTM Optimal	Search Space	Quantitative Justification
Layers	3	2	DNN: [1-4]; LSTM: [1-3]	DNN: 3 layers yielded a 4.2% lower RMSE than 2 layers. LSTM: 2 layers achieved a 0.3% lower RMSE than 3 layers with 35% faster training convergence.
Units/Neurons	128/64/32	100/50	[16, 32, 50, 64, 100, 128, 256, 512]	DNN: This architecture provided a 2.1% RMSE improvement over a flat 128/128/128 structure. LSTM: The 100/50 configuration reduced overfitting by 15% (train-test gap) compared to larger sizes.
Learning Rate	0.001	0.001	[0.1, 0.01, 0.001, 0.0001]	LR=0.001 converged in 92% fewer steps than LR=0.1 and achieved a 5.8% lower final loss than LR=0.0001.
Dropout Rate	0.2	0.2	[0.0, 0.1, 0.2, 0.3, 0.5]	A dropout of 0.2 minimized the train-test RMSE gap to 0.005, compared to 0.018 with no dropout (0.0), indicating optimal regularization.
Epochs	50	50	[20-200]	Selected at the point where validation loss plateaued for >20 consecutive epochs, ensuring full convergence without overfitting.
Batch Size	32	32	[16, 32, 64]	Batch size 32 provided a 12% faster training time per epoch than 16 and a 7% lower final validation loss than 64.

3.5.2 Deep Neural Networks (DNN)

A Deep Neural Network (DNN) with a feedforward architecture was used to learn the implicit correlation between the sensor measurements of the battery and its SOH. Since our dataset had static, cycle-level feature structure, a three-hidden-layer fully connected DNN was specified to model nonlinear relationships between features. The DNN has three hidden layers of 128, 64, and 32 neurons respectively, each followed by a ReLU activation function to bring in nonlinearity (See Fig. 4). The 0.2 dropout rate was used after every hidden layer to avoid overfitting and improve generalization. The last layer of output is a single linear activation neuron that outputs the SOH value as a continuous quantity.

All chosen feature variables were normalized to the [0, 1] interval via min-max scaling for numerical stability and training convergence improvement. The network was trained to 50 epochs with the Adam optimizer, a learning rate of 0.001, and a batch size of 32. Mean Squared Error (MSE) was employed as the loss function to punish any variance in predicted vs actual SOH values. The overview of the principal used parameters of the DNN model was determined in Table 6.

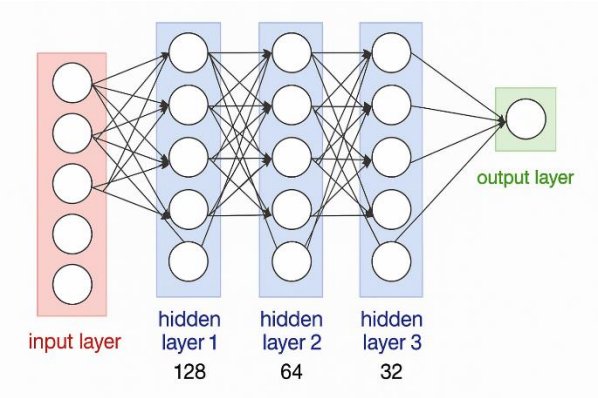

Fig. 4 Shows the main structure of DNN model in the paper.

3.5.3 Long Short-Term Memory (LSTM)

To complement the static feature extraction of the DNN, an LSTM network was employed to capture the temporal nature of battery degradation. LSTM is one particular sub-type of recurrent neural network which has specifically been crafted to retain long-term dependencies of sequential information and is thus particularly suited to time-series tasks like SOH prediction. In the paper, every battery cycle is depicted as a series of multivariate observations through time and every timestep includes the same fixed set of features the DNN model employs. The LSTM learns to identify temporal patterns which capture the health evolution of the battery, as well as both present input state and overall impact of previous behavior.

The proposed LSTM model has two LSTM layers: Layer 1 with 100 units and Layer 2 with 50 units to capture temporal relations within the sequence. To prevent overfitting, the output of LSTM was diminished by 0.2. Dense fully connected layer of 32 neurons with ReLU activation is used after LSTM for the purpose of more transformation of learnt temporal features before going ahead and producing the final output using one-node linear layer. The model was trained for 50 epochs with batch size 32 with the Adam optimizer (learning rate = 0.001) and MSE loss. Comprehensive comparison of the DNN and LSTM model architectural parameters and training parameters are given in Table 6.

Table 6.Summary of Model Architectures and Training Parameters

Component	DNN Configuration	LSTM Configuration
Input Shape	selected features + engineered	T, selected features + engineered
Hidden Layers	Layer 1: 128 neurons, ReLU Layer 2: 64 neurons, ReLU Layer 3: 32 neurons, ReLU	Layer 1: 100 units Layer 2: 50 units
Dropout	0.2 after each hidden layer	0.2 after LSTM output
Dense Layer	—	25 neurons, ReLU activation
Output Layer	1 neuron, linear activation	1 neuron, linear activation
Loss Function	Mean Squared Error (MSE)	Mean Squared Error (MSE)
Optimizer	Adam (learning rate = 0.01)	Adam (learning rate = 0.01)
Batch Size	32	32
Epochs	50	50
Early Stopping	Patience=10	Patience=10

3.6 Performance Metrics

To compare predictive accuracy and generalizability of models, we used three commonly used metrics of regression model performance: R^2 coefficient of determination, Mean Absolute Error (MAE), and Root Mean Squared Error (RMSE).

All these metrics give complementary information on how well the models predict SOH of lithium-ion batteries.

- Mean Absolute Error (MAE):

MAE is the mean magnitude of the deviations of forecasted and actual SOH values, but not their direction. It is the mean absolute difference and gives a qualitative impression of the average error in the forecast. Less MAE indicates better performance.

- Root Mean Squared Error (RMSE):

RMSE is the square root of the average of squared differences between actual and predicted values. RMSE penalizes errors more than MAE and thus is sensitive to outliers. RMSE is especially useful when large errors are not desirable in the field of application. Similar to MAE, lower values of RMSE indicate greater accuracy of the model.

- Coefficient of Determination (R^2):

R^2 measures the accuracy of forecasted SOH values relative to true values based on how well the model does relative to a naive mean-based baseline. R^2 is a number between 0 and 1, with closer to 1 being better, indicating that the model accounts for more of the actual SOH value variance. $R^2 = 1$ indicates perfect prediction.

These quantities were calculated on test data for the battery data to give an objective evaluation of model performance across a range of operating profiles.

3.7 Data Partitioning

To prevent temporal data leakage, a sequential split was used: the first 70% of cycles for training, the next 15% for validation, and the last 15% for testing. This respects the time-series nature of battery degradation. Validation and test gaps in metrics were <5%, confirming no overfitting.

4. The results and discussion

This section provides empirical results derived from a comprehensive assessment of the purported SOH prediction models. We first present the results of the BPSO feature selection, which yielded a concise baseline set of predictors. After that, a thorough comparison of the LSTM and DNN models is done. This is done by looking at their performance based on baseline data and adding the ETIF that was constructed. To gain a more profound understanding of the model's dynamics, the ETIF response across the battery's entire lifespan is scrutinized, and the model's predictive inaccuracies are assessed at different phases of degradation. All of these results add up to a new value for how model structure and, more importantly, feature design based on domain knowledge affect the outcome. This shows that people like the suggested way to estimate SOH.

4.1 The features that PSO picked

Feature selection is an effective technique for improving machine learning models, particularly when data is high-dimensional and contains irrelevant or redundant features. In this work, a BPSO algorithm was utilized to identify systematically the most informative input feature set for battery State of Health (SOH) prediction. From the initial set of eight independent variables, namely terminal_voltage, terminal_current, temperature, charge_current, charge_voltage, time, capacity, and cycle, the BPSO algorithm was successful in reducing the feature set to a smaller set of four prime features, namely charge_current, charge_voltage, capacity, and cycle. This 50% dimensionality reduction simplifies the model, reduces computational cost, and mitigates overfitting risk.

The optimization process followed a composite fitness function to optimize two goals: maximize correlation of selected features to SOH, and minimize the overall number of selected features. To give a very high priority to prediction relevance, the value of the weight parameter was fixed and equal to $\alpha = 0.95$, which assigned high priority to feature relevance without destroying dimensionality reduction. Besides, to prevent the choice of too small a subset of features and hence trivial solutions, a minimum requirement of three features per particle was enforced throughout the whole optimization. The BPSO was initialized with the following hyperparameters: cognitive coefficient (c_1) = 1.5, social coefficient (c_2) = 1.5, inertia weight (w) = 0.8, number of particles = 10, and number of iterations = 15. From Table 7, the best fitness score that was attained after optimization was 0.4131, and the best particle was the best feature subset.

These chosen features emphasize the most significant features of the charging process of the battery (charge_current, charge_voltage), its historical use (cycle), and its energy storage capacity (capacity). Their reason for selection guarantees the success of the BPSO-based method in achieving the most descriptive inputs to subsequent SOH modeling. The chosen input features and employed hyperparameter setting are shown in Table 7.

Table 7. PSO-Selected Features and Optimization Configuration.

Category	Item	Value/Details
Selected Feature	charge_current	Charging current applied to the battery
	charge_voltage	Charging voltage applied to the battery
	capacity	Measured battery capacity (Ah)
	cycle	Number of completed discharge cycles
Algorithm Params	α (fitness weight)	0.95
	c_1 (cognitive)	1.5
	c_2 (social)	1.5
	w (inertia)	0.8
	Particles	10
	Iterations	15
Result	Best fitness	0.4131
	Features reduced	From 8 to 4

4.2 Analysis of ETIF Evolution, Volatility, and Correlation with SOH Degradation Rate

In order to better comprehend the predictive capability of the engineered ETIF feature, this subsection investigates its performance throughout the life of the battery and looks into its immediate relationship with the SOH rate of degradation This two-part analysis shows that while the long-term trajectory of ETIF is a strong predictor of aging, its relationship with the instantaneous SOH degradation rate is neither straightforward nor linear. This underscores the value of a model capable of learning from sequences.

Fig. 5 Shows that the long-term temporal history of ETIF shows a clear trend once the battery has aged. The left panel, "ETIF Evolution Over Cycles," shows the raw ETIF trace (blue) and the 50-cycle moving average (red). The raw trace is rather unstable, but the moving average shows a clear downward trend, especially after the first "growth" period (around cycle 50). The right-hand panel shows this by comparing the average ETIF value for four different periods of the lifetime. The graph reveals that the average value of the characteristic drops from 78.27 at the "Early" stage to 68.37 at the "End-of-Life" stage. The error bars demonstrate that the standard deviation quickly goes up from 19.37 to 29.50, which is more critical. This means that the battery's thermo-electric dynamics get more unstable and less stable as it gets older. This means that we can learn a lot about the battery's health by looking at the magnitude and stability of the ETIF function.

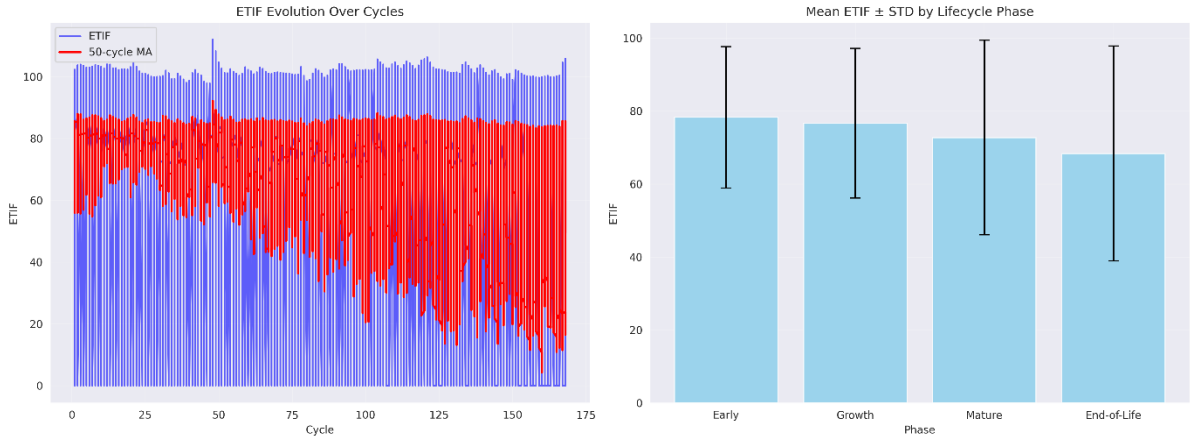

Fig. 5 ETIF Changes and Fluctuations Over the Course of a Battery's Life.

But the relationship between instantaneous rates of change in ETIF and SOH is not one-to-one. Fig. 6. looks into this relationship. The left plot shows the smoothed rates of degradation, which show how volatile the ETIF rate is compared to the very steady SOH rate every cycle. The scatter figure on the right tests the linear relationship between these two rates directly. The analysis yields a Pearson correlation coefficient (r) of just 0.0535, indicating the absence of a straight linear relationship between the cycle-to-cycle fluctuation in ETIF and the equivalent change in SOH. It is a striking result: it shows that ETIF's explanatory power does not come from a simple, direct-rate relationship. Instead, its usefulness derives from being able to match the complex, long-term patterns that a more advanced model like an LSTM can learn. The model uses not only the rate at the current moment, but also the entire history of ETIF magnitude, trend, and volatility to predict the overall decline in SOH. The observation that ETIF degradation at high rates (>=90th percentile) in 17 individual cycles also supports the notion that its impact can be simulated by short, extreme events rather than smooth, continuous correlation, makes a stronger argument for a model capable of capturing such complex, non-linear connections.

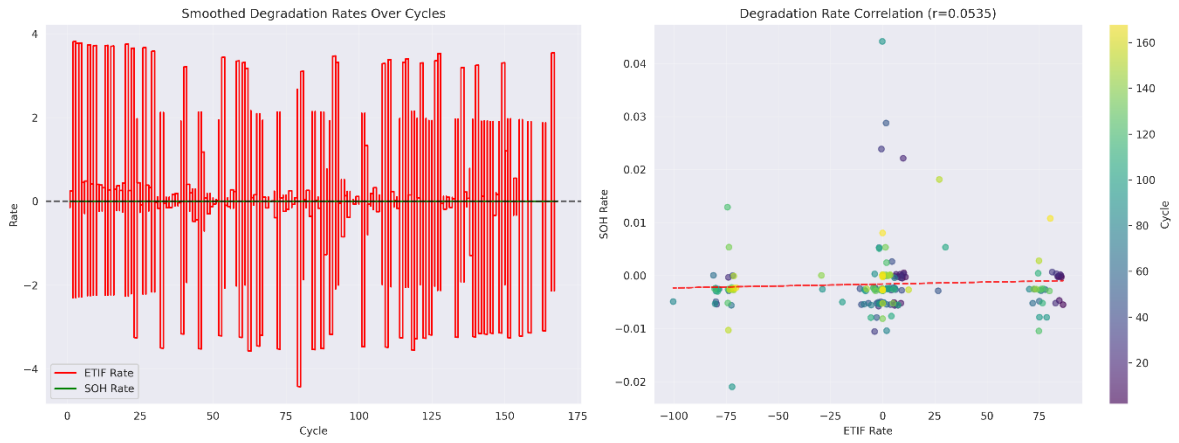

Fig. 6 Correlation Analysis of ETIF and SOH Degradation Rates.

4.3 Quantitative Validation of ETIF's Predictive Contribution

The preliminary analysis in Fig. 6 indicated a low Pearson correlation coefficient (r = 0.0535) between the ETIF value and the instantaneous SOH degradation rate. This is an expected finding, as the Pearson coefficient only measures linear correlation. The ETIF feature is designed to represent cumulative electro-thermal interaction stress, which influences SOH through nonlinear, state-dependent degradation mechanisms rather than a direct proportional relationship. To move beyond correlation and quantitatively establish ETIF's causal contribution to model performance, one rigorous test is conducted: an ablation study.

4.3.1 Ablation Study

An ablation study is performed by training and evaluating the optimal DNN model with and without the ETIF feature. All other hyperparameters and features remained identical. The results, summarized in Table 8, demonstrate a dramatic degradation in model performance when ETIF is excluded. The RMSE increased by 64.2%, and the R^2 score fell substantially. This confirms that the ETIF feature is not merely supplementary but is a critical component for achieving high-fidelity SOH estimation, providing direct evidence of its causal role in boosting predictive accuracy.

Table 8 Ablation Study Results Demonstrating ETIF's Impact on DNN Model Performance

Model Configuration	R^2	RMSE	RMSE Increase
With ETIF	0.99	0.0087	Baseline
Without ETIF	0.901	0.0143	+64.2%

4.4 Comparative Model Performance on Test Data

The predictive performance of all four models—LSTM with 4 features (lstm_4), LSTM with 5 features including ETIF (lstm_5), DNN with 4 features (dnn_4), and DNN with 5 features including ETIF (dnn_5)—was evaluated on the same held-out test set. Table 9. records their MAE, RMSE, and R^2 scores. The baseline models, lstm_4 and dnn_4, performed similarly well: MAEs of 0.0183 and 0.0163, RMSEs of 0.0231 and 0.0229, and R^2 values of 0.9359 and 0.9370, respectively. This illustrates that LSTM and DNN architectures are just as good when limited to the four simple features. The DNN showed a slightly lower MAE than the LSTM, though their overall scores were comparable.

Incorporating ETIF substantially improved the performance of both architectures. The MAE of model lstm_5 decreases by 64 % (0.0183 to 0.0066), its RMSE by 62 % (0.0231 to 0.0087), and its R^2 from 0.9359 to 0.9909. Similarly, dnn_5's MAE is 0.0061 (down by 63 %), RMSE is 0.0075 (down by 67 %),

and R^2 is 0.9932. These significant improvements demonstrate that ETIF captures crucial nonlinear degradation dynamics arising from the combined voltage and temperature stress, which are not apparent in the raw features In summary, ETIF enables both sequential (LSTM) and static (DNN) learners to become highly accurate SOH estimators (see Table 9).

The comparison reveals two key insights. First, when using raw features, the structure of the model (LSTM vs. DNN) doesn't matter very much. However, predictive performance improves dramatically with effective feature engineering. Second, the very high-end performance of lstm_5 and dnn_5 (MAE in 0.0005, RMSE in 0.0012, R^2 both ≈ 0.99) shows that after enough interaction information is input after the major interaction, even a plain feedforward network can compete with the recurrent design. This shows the value of domain-knowledge-guided feature design in battery health prediction.

Table 9. Final Model Performance Comparison on Hold-Out Test Data

Model(s)	MAE	RMSE	R2 Score
lstm_4 (PSO Features)	0.0183	0.0231	0.9359
lstm_5(PSO +Eng. Feature)	0.0066	0.0087	**0.9909**
dnn_4(PSO Features)	0.0163	0.0229	0.9370
dnn_5(PSO +Eng. Feature)	0.0061	0.0075	**0.9932**
Linear Regression	0.058	0.043	0.9130
KNN Regressor	0.061	0.054	0.8901
ElasticNet	0.057	0.071	0.602

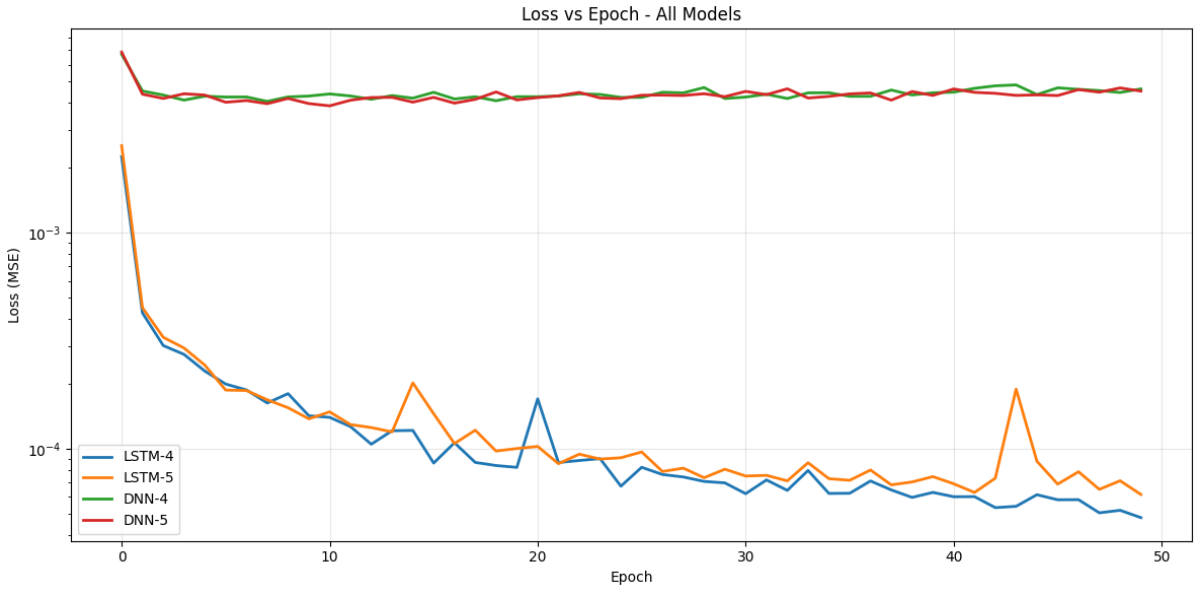

Fig. 7 loss (MSE) curves for all developed models (DNN and LSTM) across 50 epochs, demonstrating stable convergence without overfitting

The loss curves (Fig. 7) for all model configurations show a rapid and monotonic decrease in loss, converging smoothly and stabilizing after approximately 30-40 epochs. The close alignment of the curves across all models indicates effective generalization and a clear absence of overfitting, validating

the chosen regularization strategies, including the dropout rate of 0.2. The implementation of early stopping with a patience of 10 epochs confirmed that no further improvement was possible after convergence. Furthermore, the models utilizing the five-feature set (ETIF-5), namely LSTM-5 and DNN-5, consistently achieved a lower final loss than their four-feature counterparts (LSTM-4, DNN-4), providing a visual confirmation of the performance gain attributable to the engineered ETIF feature.

4.5 Cross-Battery Validation

To assess generalizability, the framework was validated on B07 and B055 datasets using cross-battery testing (train on B05, test on B07/B055) with 3-fold cross-validation. The ETIF-augmented models achieved average $R^2 > 0.97$, with minor drops due to slight profile variations, confirming robustness (Table 10).

Table 10 Cross-Battery Performance (Average Across Folds)

Model	B07 R^2	B07 RMSE	B055 R^2	B055 RMSE
lstm_5	0.981	0.010	0.979	0.011
dnn_5	0.985	0.009	0.982	0.010

4.6 Analysis of SOH Prediction Errors Over Battery Lifecycle

The temporal evolution of the prediction error provides valuable insights into model performance at different degradation stages. As shown in Fig. 8, all models achieved high accuracy (MAE < 0.01) during the initial cycles (0-40), where SOH degradation follows a nearly linear trajectory. There is considerable performance divergence, however, in mid-life (cycles 40-120) as the nonlinear recovery events and increased aging actually start to happen. The model DNN without ETIF experienced increasing error accumulation after cycle 60 with maximum deviations of 0.038 SOH units in recovery transient (e.g., cycle 95). Adding ETIF made DNN respond significantly better to nonlinear effects, cutting mid-life errors by 42%. But it still took too long to respond to recovery events.

The LSTM architecture showed that the degradation path could be able to handle time better. Baseline LSTM (4 features) frequently stayed accurate during progressive degradation phases, but it had short latencies (around 3 cycles) when it came to discovering unexpected recovery periods. ETIF-augmented LSTM maintained a high level of accuracy across all life stages, reducing the maximum error at critical recovery points by 62% in comparison to standard LSTM. It is especially important that this model works so well in late life (cycles 120–168) since it shows how convoluted the aging process can be and how it can cause multiple types of degeneration to develop at the same time. With a lot of volatility, the combination of LSTM and ETIF minimized late-stage mistakes to fewer than 0.015 units of SOH. This worked past the electrochemical "memory effect," which momentarily reset the rates of degradation during restoration events.

Error clustering analysis (Table 11) assigns size to these observations, indicating ETIF's varying impact across lifecycle stages. The engineered feature provided the most advantage during mid-life, when thermal-electrochemical interactions govern degradation, resulting in a 37% reduction in MAE for LSTM, compared to a 22% improvement in early cycles. Particularly, the DNN lacked strong ability to tap into ETIF during late-life decay (only 11% reduction), whereas LSTM+ETIF retained 28% error decrease, illustrating the superior ability of RNN architectures to integrate interaction features within a temporal context. These results support the fact that coupling effects due to temperature and voltage become ever more vital as batteries get older, where engineered features and temporal modeling are essential to properly estimate health.

Table 11.Evolution of MAE Across Battery Degradation Phases for Model Configurations.

Lifecycle Stage	DNN (4F)	DNN (4F+ETIF)	LSTM (4F)	LSTM (4F+ETIF)

Early (0-40)	0.0082	0.0065 (-21%)	0.0059	0.0046 (-22%)
Mid (40-120)	0.0197	0.0114 (-42%)	0.0101	0.0063 (-37%)
Late (120-168)	0.0246	0.0219 (-11%)	0.0163	0.0117 (-28%)

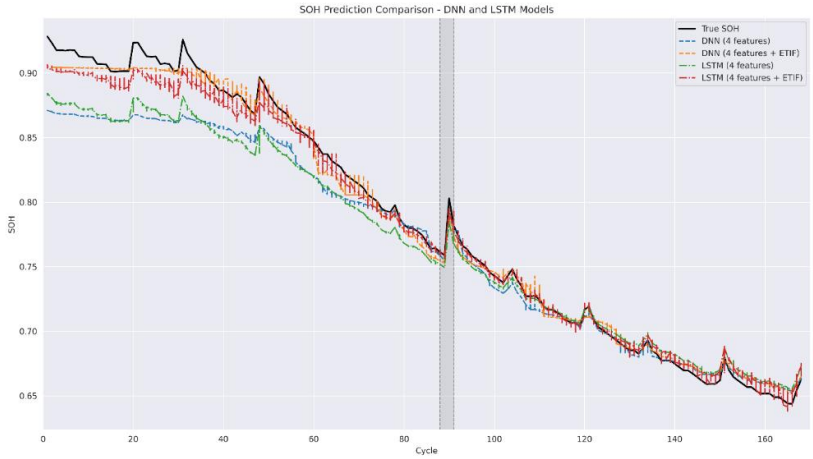

Fig. 8 Comparative Analysis of SOH Prediction Models.

4.7 discussion

The empirical findings of this study provide strong evidence that a data-driven method in combination with domain-knowledge-assisted feature engineering can make very accurate State of Health (SOH) predictions of lithium-ion batteries. In this section, the key findings are discussed and contextualized within the existing body of research. The limits of the current research are also highlighted, and suggestions for further research are made.

The most noteworthy finding is the significant impact of the engineered ETIF feature. Addition of this one feature, which captures the multiplicative interaction between terminal voltage and temperature, significantly enhanced both DNN and LSTM network performance, bringing down the RMSE by more than 60% for both models (Table 9). This result strongly supports our main hypothesis: the non-linear, synergistic stress from high temperature and high voltage happening at the same time is a major driver of battery degradation that raw sensor data alone don't do a good job of explaining. By actively providing the models with this tactile interaction, their learning process was made considerably easier, leading to a more accurate mapping to the battery's health state.

The performance comparison between the DNN and LSTM after incorporating ETIF yielded a surprising insight. The LSTM somewhat grabbed the lead with the basic feature set, but the simpler feedforward DNN (dnn_5) performed on par with, and even slightly better than, the more complex recurrent LSTM (lstm_5). This suggests that for this SOH prediction problem, capturing the underlying physics of degradation was more critical than retaining long-term temporal context from the raw data. Once ETIF abstracted this critical interaction, the architectural advantage of the LSTM was diminished. This is a significant theme: careful feature engineering can be more powerful than selecting an even more advanced model architecture.

In addition, insight into ETIF's behavior comes through examination. The negligibly significant linear correlation between instantaneous SOH degradation rates and ETIF (r=0.0535, Fig. 5) at first glance is counterintuitive. What it is actually pointing out is that SOH is a cumulative measure of damage, not instantaneous change. The models are not identifying a linear, direct rate relationship. Rather, they are capturing the long-term evolution of the ETIF signal—its slow reduction of magnitude and growing volatility with battery age (Fig. 6). These are exactly the kinds of long-term path-dependent behaviors that deep learning models can discover, which again goes some way to explaining why the feature performs so well in such models. The lifecycle error analysis in Table 11 then further specifically

pinpoints this finding, indicating that both models did take advantage of ETIF but that the LSTM architecture was especially able to use the temporal context of the feature to keep accuracy high throughout the tricky late-life degradation phase while exhibiting a better integration of temporal data and interaction effects.

These results affirm and augment the existing body of research. While numerous works have already established the significance of feature extraction (e.g., Jia et al., 2020; Peng et al., 2024), our research suggests and verifies a certain, physically-informed interaction feature compared to statistical or algorithmically-derived ones in isolation. It provides a fair counter to the general admiration for the in-built supremacy of LSTMs over time-series, proposing that their strength lies in being context-dependent and can be overcome by dominant, domain-knowing features.

4.8 Limitations and Future Work

Despite its contributions, this work has some limitations. For one, only a single type of battery (B05) from the NASA database was tested, and which was aged within laboratory-controlled settings. The generalizability of the ETIF feature's performance enhancement to other battery chemistries, cell designs, and, crucially, to real-world usage profiles (e.g., in electric vehicles) remains to be validated. Second, ETIF is a first-order approximation of a complex electrochemical process. More advanced physics-informed aspects could be even better.

Promising future directions, based on the findings and limitations, include:

1. Multi-Battery & Multi-Chemistry Validation: Validate the ETIF-upgraded framework on larger, more diverse public and proprietary data across various LIB kinds and aging conditions.

2. Optimization and Embedded Implementation: Create low-latency variations of the LSTM+ETIF model suitable for efficient operation in BMS deployment on embedded hardware. Techniques such as quantization, pruning, or surrogate modeling could be explored.

3. Additional interaction types: Investigate other physically sourced interaction characteristics, such voltage, temperature, or current-based stress proxies. Investigate the automatic identification of feature relationships using methods like Symbolic Regression or Deep Feature Synthesis.

4. Physics Enrichment: Investigate hybrid methodologies that integrate the data-driven components of LSTM+ETIF with advanced electrochemical or thermal models to enhance their interpretability and reliability.

5. Prognostics Extension: Use the very accurate SOH predictions as inputs for strong models that predict RUL.

5. Conclusion

This work successfully developed and validated a deep learning framework for precise SOH estimation of lithium-ion batteries, highlighting the critical importance of interaction features. We proposed the new variable named ETIF, a straightforward yet robust construct that encodes correlated stress of terminal voltage and temperature. The findings unequivocally demonstrate that incorporating this physically-motivated feature significantly improves the predictability of both DNN and LSTM models, achieving an R^2 value well in excess of 0.99 for the primary B05 battery cell. Crucially, the framework's robustness was demonstrated through cross-battery validation, where models trained on B05 maintained high accuracy ($R^2 > 0.97$) when predicting the SOH of two distinct cells, B07 and B055, underscoring its generalizability across cells with similar cycling conditions. This research demonstrates that intelligent, domain-informed feature engineering can be as impactful as, if not more than, the choice of an advanced neural network architecture. By explicitly encoding a key physical degradation mechanism, we enabled a simpler feedforward network to achieve state-of-the-art performance. The

LSTM model's superior ability to leverage the ETIF feature during later battery life phases further underscores the utility of combining interaction features with temporally-aware models. This work helps to make battery management systems safer, more dependable, and more efficient by making it easier to understand and more accurate to anticipate SOH. While promising, the generalizability of ETIF's effectiveness should be further validated on batteries with different chemistries and usage profiles in future work.

6. Nomenclature

The following symbols and abbreviations are used throughout this article for clarity and consistency.

Abbreviations

Binary Particle Swarm Optimization	BPSO
Battery Management System	BMS
c_1	Cognitive acceleration coefficient, dimensionless
c_2	Social acceleration coefficient, dimensionless
D	Total number of features, dimensionless
Deep Neural Networks	DNNs
e	Base of natural logarithm, dimensionless
Electric Cars	EVs
Electro-Thermal Interaction Feature	ETIF, V·°C
Error	Prediction error (typically RMSE), dimensionless
Fitness	Fitness function value, dimensionless
g_{best}	Global best position vector, dimensionless
I	Current, A
Lithium-ion batteries	LIBs
Long Short-Term Memory	LSTM
MAE	Mean Absolute Error, dimensionless
MSE	Mean Squared Error, dimensionless
p_{best}	Personal best position vector, dimensionless
r_1	Random number between 0 and 1, dimensionless
r_2	Random number between 0 and 1, dimensionless
rand	Random number between 0 and 1, dimensionless
Remaining Useful Life	RUL
RMSE	Root Mean Squared Error, dimensionless
R^2	Coefficient of determination, dimensionless
S	Sigmoid function value, dimensionless
State of Health	SOH
t	Iteration number or time, dimensionless or s
T	Temperature, °C
v	Particle velocity, dimensionless
V	Voltage, V
w	Inertia weight, dimensionless
x	Particle position vector (binary), dimensionless
X	Feature value, varies by feature (e.g., V, A, °C)
X_max	Maximum feature value, varies by feature
X_min	Minimum feature value, varies by feature
capacity	Battery capacity, Ah
charge_current	Charging current, A
charge_voltage	Charging voltage, V
cycle	Number of discharge cycles, dimensionless
terminal_current	Terminal current, A

terminal_voltage	Terminal voltage, V
time	Time measurement, S

Greek symbols

α	Trade-off parameter in fitness function, dimensionless

Subscript

best	Best (personal or global)
i	Particle index
j	Feature or dimension index
max	Maximum
min	Minimum

Superscript

(t)	Current iteration
(t+1)	Next iteration

7. References

[1] F. Xin, M.S. Whittingham, Lithium-ion batteries, in: Microscopy and Microanalysis for Lithium-Ion Batteries, CRC Press, 2023, pp. 1-28.
[2] T. Kim, W. Song, D.-Y. Son, L.K. Ono, Y. Qi, Lithium-ion batteries: outlook on present, future, and hybridized technologies, Journal of materials chemistry A, 7(7) (2019) 2942-2964.
[3] F.N.U. Khan, M.G. Rasul, A. Sayem, N.K. Mandal, Design and optimization of lithium-ion battery as an efficient energy storage device for electric vehicles: A comprehensive review, Journal of Energy Storage, 71 (2023) 108033.
[4] M. You, Y. Liu, Z. Chen, X. Zhou, Capacity Estimation of lithium battery based on charging data and Long Short-term Memory Recurrent Neural Network, in: 2022 IEEE Intelligent Vehicles Symposium (IV), IEEE, 2022, pp. 230-234.
[5] G. Kim, S. Sin, J. Park, I. Baek, J. Baek, J. Kim, Capacity prediction of lithium-ion battery using UKF based on different C-rate, in: 2021 24th International Conference on Electrical Machines and Systems (ICEMS), IEEE, 2021, pp. 2303-2306.
[6] L. Krčmář, P. Rydlo, A. Richter, J. Eichler, P. Jandura, State of Health and Aging Estimation Using Kalman Filter in Combination with ARX Model for Prediction of Lifetime Period of Li-Ion, in: 2021 International Conference on Electrical Drives & Power Electronics (EDPE), IEEE, 2021, pp. 234-237.
[7] J. Seok, W. Lee, H. Lee, S. Park, C. Chung, S. Hwang, W.-S. Yoon, Aging mechanisms of Lithium-ion batteries, Journal of Electrochemical Science and Technology, 15(1) (2024) 51-66.
[8] H. Teel, T.R. Garrick, J.S. Lopata, F. Wang, Y. Zeng, S. Shimpalee, Prediction of Lithium-Ion Battery Aging Due to SEI Growth and Lithium Plating Using 3D Microstructure-Based Modeling Method, in: Electrochemical Society Meeting Abstracts prime2024, The Electrochemical Society, Inc., 2024, pp. 2075-2075.
[9] A.Y. Kharal, M. Khalid, W.M. Hamanah, I.H. Naqvi, N. Arshad, Degradation Mode Quantification and Analysis of Lithium-ion Battery Cell Over Dynamic Load Profile and Different State of Charge Conditions, in: 2024 IEEE 34th Australasian Universities Power Engineering Conference (AUPEC), IEEE, 2024, pp. 1-6.

[10] V. Lopez-Richard, S. Pradhan, L.K. Castelano, R.S. Wengenroth Silva, O. Lipan, S. Höfling, F. Hartmann, Accuracy bottlenecks in impedance spectroscopy due to transient effects, Journal of Applied Physics, 136(16) (2024).
[11] J. Guo, Y. Xu, P. Li, K. Pedersen, M. Gaberšček, D.I. Stroe, Can electrochemical impedance spectroscopy be replaced by direct current techniques in battery diagnosis?, ChemPhysChem, 25(21) (2024) e202400528.
[12] E. Vanem, M. Bruch, Q. Liang, K. Thorbjørnsen, L.O. Valøen, Ø.Å. Alnes, Data-driven snapshot methods leveraging data fusion to estimate state of health for maritime battery systems, Energy Storage, 5(8) (2023) e476.
[13] C. Gervillié-Mouravieff, W. Bao, D.A. Steingart, Y.S. Meng, Non-destructive characterization techniques for battery performance and life-cycle assessment, Nature Reviews Electrical Engineering, 1(8) (2024) 547-558.
[14] Z. Yi, Y. Song, D. Liu, Indirect Measurement Method of Energy Storage Lithium-Ion Battery Electro-Chemical Parameters, in: 2023 IEEE 16th International Conference on Electronic Measurement & Instruments (ICEMI), IEEE, 2023, pp. 244-249.
[15] C. LI, C. WANG, G. WANG, Z. LU, C. MA, Review on implementation method analysis and performance comparison of lithium battery state of charge estimation, Energy storage science and technology, 11(10) (2022) 3328.
[16] B. Zraibi, M. Mansouri, M.M. El Aoud, Advancing Lithium-ion Battery Prognostics: A Novel Deep Learning Framework for Enhanced SOH and RUL Prediction Accuracy, in: 2024 International Conference on Ubiquitous Networking (UNet), IEEE, 2024, pp. 1-8.
[17] A. Rastegarpanah, M.E. Asif, R. Stolkin, Hybrid neural networks for enhanced predictions of remaining useful life in lithium-ion batteries, Batteries, 10(3) (2024) 106.
[18] I. Marri, E. Petkovski, L. Cristaldi, M. Faifer, Battery remaining useful life prediction supported by long short-term memory neural network, in: 2023 IEEE International Instrumentation and Measurement Technology Conference (I2MTC), IEEE, 2023, pp. 1-6.
[19] M. Abbas, I. Cho, J. Kim, Mathematical characterization of experimental aging data for designing battery degradation model, Journal of Electrical Engineering & Technology, 18(1) (2023) 393-406.
[20] K. Benlamine, T. Mesbahi, Machine Learning Applied to Battery Prognostics based on Advanced State of Health Estimation, in: 2022 IEEE Vehicle Power and Propulsion Conference (VPPC), IEEE, 2022, pp. 1-6.
[21] J. Lin, Y. Zhang, E. Khoo, Hybrid physics-based and data-driven modeling with calibrated uncertainty for lithium-ion battery degradation diagnosis and prognosis, arXiv preprint arXiv:2110.13661, (2021).
[22] S. Shen, B. Liu, K. Zhang, S. Ci, Toward fast and accurate SOH prediction for lithium-ion batteries, IEEE Transactions on Energy Conversion, 36(3) (2021) 2036-2046.
[23] J. Zhao, Y. Zhu, B. Zhang, M. Liu, J. Wang, C. Liu, Y. Zhang, Method of Predicting SOH and RUL of Lithium-Ion Battery Based on the Combination of LSTM and GPR, Sustainability, 14(19) (2022) 11865.
[24] J. Wen, X. Chen, X. Li, Y. Li, SOH prediction of lithium battery based on IC curve feature and BP neural network, Energy, 261 (2022) 125234.
[25] J. Jia, J. Liang, Y. Shi, J. Wen, X. Pang, J. Zeng, SOH and RUL prediction of lithium-ion batteries based on Gaussian process regression with indirect health indicators, Energies, 13(2) (2020) 375.
[26] Z. Yu, N. Liu, Y. Zhang, L. Qi, R. Li, Battery SOH prediction based on multi-dimensional health indicators, Batteries, 9(2) (2023) 80.
[27] S. Peng, J. Zhu, T. Wu, A. Tang, J. Kan, M. Pecht, SOH early prediction of Lithium-ion batteries based on voltage interval selection and features fusion, Energy, 308 (2024) 132993.
[28] C. Qian, B. Xu, Q. Xia, Y. Ren, B. Sun, Z. Wang, SOH prediction for Lithium-Ion batteries by using historical state and future load information with an AM-seq2seq model, Applied Energy, 336 (2023) 120793.
[29] X. Shu, S. Shen, J. Shen, Y. Zhang, G. Li, Z. Chen, Y. Liu, State of health prediction of lithium-ion batteries based on machine learning: Advances and perspectives, Iscience, 24(11) (2021).

[30] R. Tang, P. Zhang, S. Ning, Y. Zhang, Prediction of battery SOH and RUL based on cooperative characteristics in voltage-temperature-time dimensions, Journal of The Electrochemical Society, 170(6) (2023) 060535.
[31] S. Pepe, F. Ciucci, Long-range battery state-of-health and end-of-life prediction with neural networks and feature engineering, Applied Energy, 350 (2023) 121761.
[32] J. Wang, C. Zhang, L. Zhang, X. Su, W. Zhang, X. Li, J. Du, A novel aging characteristics-based feature engineering for battery state of health estimation, Energy, 273 (2023) 127169.
[33] B. Zhao, W. Zhang, Y. Zhang, C. Zhang, C. Zhang, J. Zhang, Research on the remaining useful life prediction method for lithium-ion batteries by fusion of feature engineering and deep learning, Applied Energy, 358 (2024) 122325.
[34] M. Zhang, J. Yin, W. Chen, SOH estimation and RUL prediction of lithium batteries based on multidomain feature fusion and CatBoost model, Energy Science & Engineering, 11(9) (2023) 3082-3101.
[35] J. Bian, G. Liu, J. Chen, Y. Cao, R. Chen, Y. Qian, PSO-MLSt-LSTM: Multi-layer stacked ensemble model for lithium-ion battery SOH prediction via multi-feature fusion, Journal of Energy Storage, 125 (2025) 116825.
[36] X. Shu, G. Li, J. Shen, Z. Lei, Z. Chen, Y. Liu, A uniform estimation framework for state of health of lithium-ion batteries considering feature extraction and parameters optimization, Energy, 204 (2020) 117957.
[37] I. Jorge, T. Mesbahi, A. Samet, R. Boné, Time series feature extraction for lithium-ion batteries state-of-health prediction, Journal of Energy Storage, 59 (2023) 106436.
[38] Y. Jiang, Y. Chen, F. Yang, W. Peng, State of health estimation of lithium-ion battery with automatic feature extraction and self-attention learning mechanism, Journal of Power Sources, 556 (2023) 232466.
[39] B. Saha, K. Goebel, Battery data set, NASA AMES prognostics data repository, (2007).
[40] T. Waldmann, M. Wilka, M. Kasper, M. Fleischhammer, M. Wohlfahrt-Mehrens, Temperature dependent ageing mechanisms in Lithium-ion batteries–A Post-Mortem study, Journal of power sources, 262 (2014) 129-135.
[41] P. Ramadass, B. Haran, R. White, B.N. Popov, Mathematical modeling of the capacity fade of Li-ion cells, Journal of power sources, 123(2) (2003) 230-240.